

# UC San Diego

## UC San Diego Previously Published Works

### Title

Investigating Intrinsically Disordered Proteins With Brownian Dynamics

### Permalink

<https://escholarship.org/uc/item/11z7q53b>

### Authors

Ahn, Surl-Hee  
Huber, Gary A  
McCammon, J Andrew

### Publication Date

2022

### DOI

10.3389/fmolb.2022.898838

Peer reviewed



# Investigating Intrinsically Disordered Proteins With Brownian Dynamics

Surl-Hee Ahn<sup>1\*†</sup>, Gary A. Huber<sup>1,2†</sup> and J. Andrew McCammon<sup>1,2</sup>

<sup>1</sup>Department of Chemistry and Biochemistry, University of California, San Diego, San Diego, CA, United States, <sup>2</sup>Department of Pharmacology, University of California, San Diego, San Diego, CA, United States

Intrinsically disordered proteins (IDPs) have recently become systems of great interest due to their involvement in modulating many biological processes and their aggregation being implicated in many diseases. Since IDPs do not have a stable, folded structure, however, they cannot be easily studied with experimental techniques. Hence, conducting a computational study of these systems can be helpful and be complementary with experimental work to elucidate their mechanisms. Thus, we have implemented the coarse-grained force field for proteins (COFFDROP) in Browndye 2.0 to study IDPs using Brownian dynamics (BD) simulations, which are often used to study large-scale motions with longer time scales and diffusion-limited molecular associations. Specifically, we have checked our COFFDROP implementation with eight naturally occurring IDPs and have investigated five (Glu-Lys)<sub>25</sub> IDP sequence variants. From measuring the hydrodynamic radii of eight naturally occurring IDPs, we found the ideal scaling factor of 0.786 for non-bonded interactions. We have also measured the entanglement indices (average C<sub>α</sub> distances to the other chain) between two (Glu-Lys)<sub>25</sub> IDP sequence variants, a property related to molecular association. We found that entanglement indices decrease for all possible pairs at excess salt concentration, which is consistent with long-range interactions of these IDP sequence variants getting weaker at increasing salt concentration.

**Keywords:** Brownian dynamics simulation, molecular associations, intrinsically disordered proteins, COFFDROP force field, Browndye

## OPEN ACCESS

### Edited by:

Alexey V. Onufriev,  
Virginia Tech, United States

### Reviewed by:

Stefano Piana-Agostinetti,  
D. E. Shaw Research, United States  
Jung-Hsin Lin,  
Academia Sinica, Taiwan

### \*Correspondence:

Surl-Hee Ahn  
s3ahn@ucsd.edu

<sup>†</sup>These authors have contributed  
equally to this work

### Specialty section:

This article was submitted to  
Molecular Recognition,  
a section of the journal  
Frontiers in Molecular Biosciences

**Received:** 17 March 2022

**Accepted:** 17 May 2022

**Published:** 08 June 2022

### Citation:

Ahn S-H, Huber GA and  
McCammon JA (2022) Investigating  
Intrinsically Disordered Proteins With  
Brownian Dynamics.  
Front. Mol. Biosci. 9:898838.  
doi: 10.3389/fmolb.2022.898838

## 1 INTRODUCTION

One of the main determinants of biological structure and function is the interaction of two or more molecules, especially protein molecules. Understanding the dynamics of these bimolecular interactions is important for the understanding of such cellular structures as the cytoskeleton (actin and tubulin, for example), ribosomes, chromosomes, and polymerases, as well as processes such as cell signaling and cell motility (Alberts et al., 2002; Pollard and Earnshaw, 2007). Furthermore, the encounter stages of such reactions, which are often the rate-limiting steps, are diffusion-limited (Elcock, 2004). Therefore, the use of Brownian dynamics (BD) is appropriate for such systems [see Huber and McCammon (2019) for a review]. For several decades, BD has found use in polymer and peptide simulations, simulations of enzyme-substrate reactions, and protein-protein association reactions. More recently BD has found use in studies of large-scale cytoplasm simulations, microtubule dynamics, assembly of protein complexes, retroviral infectivity, molecular motors, chromosome organization, the nuclear pore complex, synapses, and endocytosis. The previous version of the Browndye software package (Browndye 1.0), which was limited to two

rigid bodies, has been used in enzyme kinetics and channeling (Huang et al., 2018), as well as protein-protein interactions (Grant et al., 2011).

The Browndye 2.0 software package, successor to the previous simulation package, consists of two simulation programs and about 38 auxiliary programs for processing data. Like the previous version, Browndye 2.0 can compute the second-order rate constants of the encounter of two bodies moving according to BD, compute the probabilities of the two bodies moving from one binding mode to another, and output the molecules' trajectories. The main addition is the ability to model each molecule as a collection of large rigid cores with flexible connectors and loops. In its original two-rigid-body model, Browndye has functionality very similar to the packages SDA (Martinez et al., 2015), MacroDox (Northrup et al., 1993), and GeomBD (Roberts and Chang, 2016), and is intended primarily for simulations of large biological molecules like those three other packages. Its current limitations arise mainly from the structural rigidity approximations and the nature of the force computations between the molecules.

Using Browndye 2.0, we have investigated intrinsically disordered proteins (IDPs), which are proteins that do not have a stable, folded structure and instead take on various structures depending on their current tasks in modulating biological processes. Conducting a computational study of these systems will be critical to elucidate their mechanisms. Specifically, we have implemented the coarse-grained force field for proteins (COFFDROP) (Andrews and Elcock, 2014; Frembgen-Kesner et al., 2015) in Browndye 2.0 to study eight naturally occurring IDPs and five (Glu-Lys)<sub>25</sub> IDP sequence variants. We have measured their structural properties, including radius of gyration ( $R_g$ ), interresidue distances ( $R_{ij}$ ), and hydrodynamic radius ( $R_h$ ), and a property related to molecular association, namely the entanglement index (average  $C_\alpha$  distance to the other chain).

## 2 MATERIALS AND METHODS

### 2.1 Structure Preparation

The AlphaFold Colab (Jumper et al., 2021) was used to prepare the starting structures for the five (Glu-Lys)<sub>25</sub> IDP sequence variants and eight naturally occurring IDPs that were used in Frembgen-Kesner et al. (2015), which are Alzheimer amyloid  $\beta_{(1-40)}$  ( $A\beta_{(1-40)}$ ) (Danielsson et al., 2002), suppressor of Mec1 lethality (Sml1) (Danielsson et al., 2008), *Lotus japonicas* intrinsically disordered protein 1 (*LjIDP1*) (Haaning et al., 2008), prothymosin  $\alpha$  (ProT $\alpha$ ) (Yi et al., 2007), abscisic acid stress ripening 1 (ASR1) (Goldgur et al., 2007), yeast nucleoporin 116 (Nup116) (Krishnan et al., 2008),  $\alpha$ -synuclein (Uversky et al., 2001), and cystic fibrosis transmembrane conductance regulator regulatory region (CFTR R) (Baker, 2009). We have used AlphaFold to prepare the starting structures for the naturally occurring IDPs since they have conditionally folded regions that have confident per-residue confidence scores (pLDDT) (above 70 in a range from 0 to 100), which are expected to be accurately predicted by AlphaFold (Alderson et al., 2022). We have also used

```
sv10
EKKKKKKKEEKKKEEEEEKKEEKKKEKKEEKEEKEKKEKKEEKEE
sv15
KKEKKEKKEKKEKKEEKEKKEKKEKKEKKEEKEEKEEKEEKEE
sv20
EEKEEEEEEKEEKEEKEEKEEKEEKEEKEEKEEKKKKKKKKKKKEE
sv25
EEEEEEEEEEKEEKEEKEEKEEKKKKKKKKKKKKKKKKKKKEEKEE
sv30
EEEEEEEEEEEEEEEEEEEEEEEEEEEEKKEEKEEKEEKEEKEEKEE
```

**FIGURE 1** | The five (Glu-Lys)<sub>25</sub> IDP sequence variants used in the study. Glutamic acid (E) is colored in red for negative charge, and lysine (K) is colored in blue for positive charge. The labels for the sequence variants (sv) are from Das and Pappu (2013). The five sequence variants are the same ones tested in McCarty et al. (2019).

AlphaFold for the five (Glu-Lys)<sub>25</sub> IDP sequence variants since peptides composed of many Glu and Lys residues favor forming  $\alpha$ -helical structures (Marqusee and Baldwin, 1987; Iqbalsyah and Doig, 2005; Meuzelaar et al., 2016; Wolny et al., 2017), and AlphaFold had yielded  $\alpha$ -helical structures for all five IDP sequence variants.

**Figures 1, 2** show the amino acid sequences of these systems, respectively, and **Table 1** summarizes the various characteristics of the systems obtained from the classification of intrinsically disordered ensemble regions (CIDER) program (Holehouse et al., 2015).

The protonation states were assigned using PROPKA 3 (Olsson et al., 2011; Søndergaard et al., 2011) at pH 7.0 for the five (Glu-Lys)<sub>25</sub> IDP sequence variants and at appropriate pH's for the eight IDPs as done in Frembgen-Kesner et al. (2015), which are listed in the **Supplementary Material**. PDB2PQR 3.4 (Jurrus et al., 2018; Unni et al., 2011; Dolinsky et al., 2007, 2004) was used to convert the PDB files to PQR format for the BD simulations. The temperature  $T$  was set to 298 K, and the dielectric constant was set to 78.4 for all systems. For the five (Glu-Lys)<sub>25</sub> IDP sequence variants, the ionic concentration was set to NaCl 15 mM (reference concentration) or NaCl 125 mM (excess salt concentration) as done in Das and Pappu (2013) by setting the appropriate Debye length  $\lambda_D$  using **Equation 1**

$$\lambda_D = \left( \frac{\epsilon_0 \epsilon_r k_B T}{2e^2 N_A C} \right)^{1/2}, \quad (1)$$

where  $\epsilon_0$  is the permittivity of the free space,  $\epsilon_r$  is the dielectric constant (of water in this case),  $k_B$  is the Boltzmann constant,  $T$  is the temperature (298 K in this case),  $e$  is the elementary charge,  $N_A$  is Avogadro's constant, and  $C$  is the ionic strength in mol/m<sup>3</sup> units. The Debye length  $\lambda_D$  was set to be 7.85 Å for NaCl 15 mM (reference concentration) and 2.72 Å for NaCl 125 mM (excess salt concentration).

### 2.2 Brownian Dynamics Simulations

The BD simulations were run using Browndye 2.0 (Huber and McCammon, 2010) with the spline-based potential coarse-grained force field for proteins (COFFDROP) (Andrews and

**A $\beta$ <sub>(1-40)</sub>**  
**DAEFRHDSGY EVHHQKLVFF AEDVGSNKGA IIGLMVGGVV**

**Sml1**  
**MQNSQDYFYA QNRCQQQQAP STLRVTMAE FRRVPLPPMA**  
**EVPMLSTQNS MGSSASASAS SLEMWEKOLE ERLNSIDHDM**  
**NNNKFGSGEL KSMFNQGVVE EMDF**

**LjIDP1**  
**AHHHHHHVDD DDKMARSFTN IKAISALVAE EFSNSLARRG**  
**YAATAQSAGR VGASMSGKMG STKSGEEKAA AREKVSWVPD**  
**PVTGYYPEN IKEIDVAELR SAVLGKN**

**ProT $\alpha$**   
**SDAAVDTSE ITTKDLKEKK EVVEEAENGR DAPANGNANE**  
**ENGEQADNE VDEEEEEEGGE EEEEEEGDG EEDGDDEDEE**  
**AESATGKRAA EDEDDDDVDT KKQKTDEDD**

**ASR1**  
**MEEEKHHHHH LFHHKDAEE GPVDYEKEIK HHKHLEQIGK**  
**LGTVAAGAYA LHEKHEAKKD PEHAHKHKIE EEIAAAAAGV**  
**AGGFAFHEHH EKKDAKKEEK KKLRGDTTIS SKLLF**

**Nup116**  
**GSRRASVGSQ ALFGAKPASG GLFGQSAGSK AFGMNTNPTG**  
**TTGGLFGQTN QQQSGGGLFG QQQNSNAGGL FGQNNQSQNQ**  
**SGLFGQQNSS NAFGQPQQQG GLFGSKPAGG LFGQQQGAST**  
**HHHHHH**

**$\alpha$ -Synuclein**  
**MDVFMKGLSK AKEGVVAAA E KTKQGVAAE GKTKEGVLYV**  
**GSKTKEGVVH GVATVAEKTQ EQVTNVGGAV VTGVTAVAQK**  
**TVEGAGSIAA ATGFVKKDQL GKNEEGAPQE GILEDMPVDP**  
**DNEAYEMPSE EGYQDYEPEA**

**CFTR R**  
**QGAMESAERR NSILTEHLR FSLEGDAPVS WTETKKQSFK**  
**QTGEFGEKRK NSILNPINSI RKFSIVQKTP LQMNGIEEDS**  
**DEPLERRLSL VPDSQQGEAI LPRISVISTG PTLQARRRQS**  
**VLNLMTHSVN QGQNIHRKTT ASTRKVS LAP QANLTEDIY**  
**SRRLSQETGL EISEEINEED LKECLFDDME**

**FIGURE 2 |** The eight naturally occurring IDPs used in the study. Glutamic acid (E) and aspartic acid (D) are colored in red for negative charge, and lysine (K) and arginine (R) are colored in blue for positive charge. The eight IDPs are from Frembgen-Kesner et al. (2015).

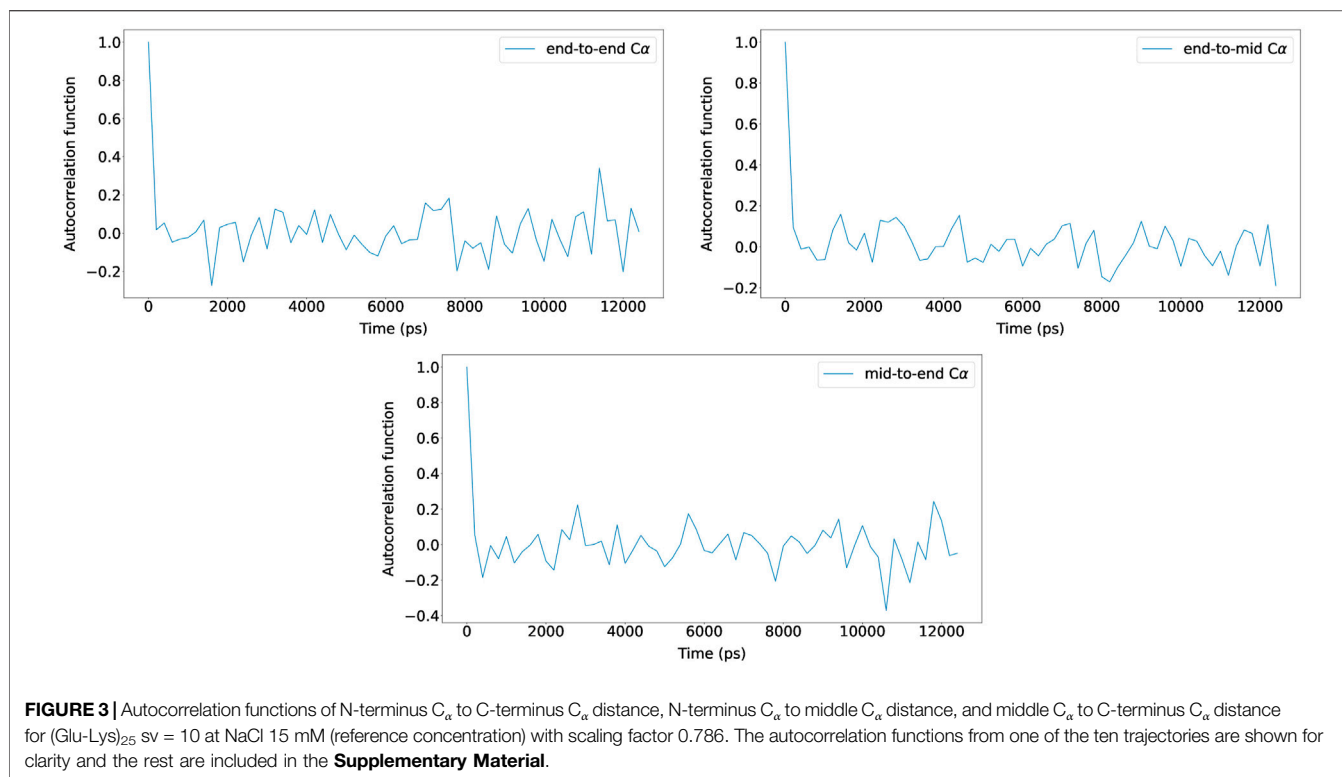
**TABLE 1 |** Summary of classification of intrinsically disordered ensemble regions (CIDER) (Holehouse et al., 2015) results for the IDPs used in the study. NCPN denotes the net charge per residue, FCR denotes the fraction of charged residues, and  $\kappa$  denotes the measure of charge segregation from Das and Pappu (2013). Hydrophathy measures how hydrophobic the sequence is (0–9 with 0 being least hydrophobic and nine being most hydrophobic) (Kyte and Doolittle, 1982) and disorder measures the fraction of disorder promoting residues (Uversky, 2002). The categorization of each IDP is determined from the Das-Pappu phase diagram (Das and Pappu, 2013; Holehouse et al., 2015).

IDP	Length	NCPN	FCR	$\kappa$	Hydrophathy	Disorder	Category
sv10	50	0.000	1.000	0.083	0.800	1.000	Strong polyampholytes
sv15	50	0.000	1.000	0.135	0.800	1.000	Strong polyampholytes
sv20	50	0.000	1.000	0.272	0.800	1.000	Strong polyampholytes
sv25	50	0.000	1.000	0.528	0.800	1.000	Strong polyampholytes
sv30	50	0.000	1.000	1.000	0.800	1.000	Strong polyampholytes
A $\beta$ <sub>(1-40)</sub>	40	-0.075	0.225	0.211	4.558	0.600	Weak polyampholytes
Sml1	104	-0.048	0.221	0.143	3.712	0.635	Weak polyampholytes
LjIDP1	107	0.009	0.271	0.174	3.890	0.729	Janus sequences
ProT $\alpha$	109	-0.394	0.578	0.424	2.507	0.881	Strong polyelectrolytes
ASR1	115	-0.017	0.383	0.100	3.326	0.809	Strong polyampholytes
Nup116	126	0.040	0.040	0.278	3.709	0.762	Weak polyampholytes
$\alpha$ -Synuclein	140	-0.064	0.279	0.172	4.097	0.729	Janus sequences
CFTR R	190	-0.026	0.289	0.285	3.743	0.679	Janus sequences

Elcock, 2014; Frembgen-Kesner et al., 2015), which was newly implemented for Browndye 2.0. In COFFDROP, each amino acid is represented as a “bead” so that a protein sequence can be represented as a flexible “chain” composed of beads. In addition, since the scaling of non-bonded interactions improved COFFDROP’s ability to reproduce experimental results (Frembgen-Kesner et al., 2015), this feature was also implemented for Browndye 2.0. Moreover in Browndye 2.0, interactions can be computed less frequently, which is useful since computing these interactions take up most of the simulation time for longer chains. Finally in Browndye 2.0, a constant time step size can be set, and the recommended value is 0.05 ps for COFFDROP chains, unless bond constraints are used in which case a larger constant time

step size is allowed, which can make the simulations run faster.

For the eight naturally occurring IDPs, the maximum number of BD simulation steps was set to 80,000,000, and a constant time step size of 0.05 ps was used (no bond constraints used). To calculate the hydrodynamic radius ( $R_h$ ) for each COFFDROP potential with a scaling factor (0.5–1.0 in intervals of 0.1) for non-bonded interactions, ten trajectories were run for each system and potential, and simulation snapshots were recorded every 200,000 steps. Hydrodynamic interactions were updated every 400 steps. The specific parameter values follow the parameter values from Frembgen-Kesner et al. (2015) since these IDPs were used to check the COFFDROP implementation for Browndye 2.0.



For the five (Glu-Lys)<sub>25</sub> IDP sequence variants, the maximum number of BD simulation steps was set to 125,000,000, and by using bond constraints, a constant time step size of 0.2 ps was used (25  $\mu$ s total). The autocorrelation functions of N-terminus C<sub>α</sub> to C-terminus C<sub>α</sub> distance, N-terminus C<sub>α</sub> to middle C<sub>α</sub> distance, and middle C<sub>α</sub> to C-terminus C<sub>α</sub> distance were measured and plotted with new BrownDye 2.0 functions chain\_atom\_distances and autocor to check whether the simulation time was sufficiently long enough to obtain converged properties. As seen in **Figure 3**, the three autocorrelation functions converge, and the simulation time was regarded to be sufficiently long enough. The rest of the autocorrelation functions are included in the **Supplementary Material**. As seen from the **Supplementary Material**, the shortest simulation was 12 ns, whereas the longest simulation was 25  $\mu$ s. To calculate structural properties such as radius of gyration ( $R_g$ ), ten trajectories were run for each system, and simulation snapshots were recorded every 100,000 steps. Hydrodynamic interactions were updated every 400 steps.

### 3 RESULTS

#### 3.1 Eight Naturally Occurring IDPs

We first investigated the eight naturally occurring IDPs to see if BrownDye 2.0 can reproduce the COFFDROP results in Frembgen-Kesner et al. (2015). In particular, we measured the hydrodynamic radius ( $R_h$ ) for each system and COFFDROP potential with a scaling factor (0.5–1.0 in intervals of 0.1) for non-bonded interactions.  $R_h$  is the radius of a hard-sphere that

diffuses at the same rate as solute and is dependent on the size and hydration of protein. The Kirkwood definition (Kirkwood, 1996) was used to calculate  $R_h$  as stated in **Equation 2**

$$\frac{1}{R_h} = \left\langle \frac{1}{r_{ij}} \right\rangle_{i \neq j} \quad (2)$$

where  $r_{ij}$  denotes pairwise distances between C<sub>α</sub> of amino acids  $i$  and  $j$ , as done in Nygaard et al. (2017).  $R_h$  was calculated for each simulation snapshot (every 200,000 steps), and the final  $R_h$  value for each simulation was obtained by averaging the  $R_h$  values from the simulation. The average  $R_h$  values, along with standard error bars (95% confidence interval), from ten independent simulations, are plotted in **Figure 4**. To match up with the COFFDROP results that used the HYDROPRO program (Ortega et al., 2011), the average  $R_h$  values and standard error bars were multiplied by 1.186 and added by 1.03 as done in Nygaard et al. (2017). The  $R_h$  values are in good agreement with those in Frembgen-Kesner et al. (2015), which are marked as dashed lines with square markers in **Figure 4**, indicating that the COFFDROP implementation in BrownDye 2.0 is reliable. The small discrepancies between the two results could be from the long-range electrostatic interactions being computed differently, i.e., Frembgen-Kesner et al. (2015) used a treecode algorithm (Li et al., 2009) that involves Taylor expansion to compute particle-cluster interactions, whereas this study used pairwise summations of potentials evaluated by a cubic spline using tabulated COFFDROP potential data. Except for ProT $\alpha$ , the ideal scaling factor for the naturally occurring IDPs is between 0.7 and 0.8, which allows the BD simulation results to match up with



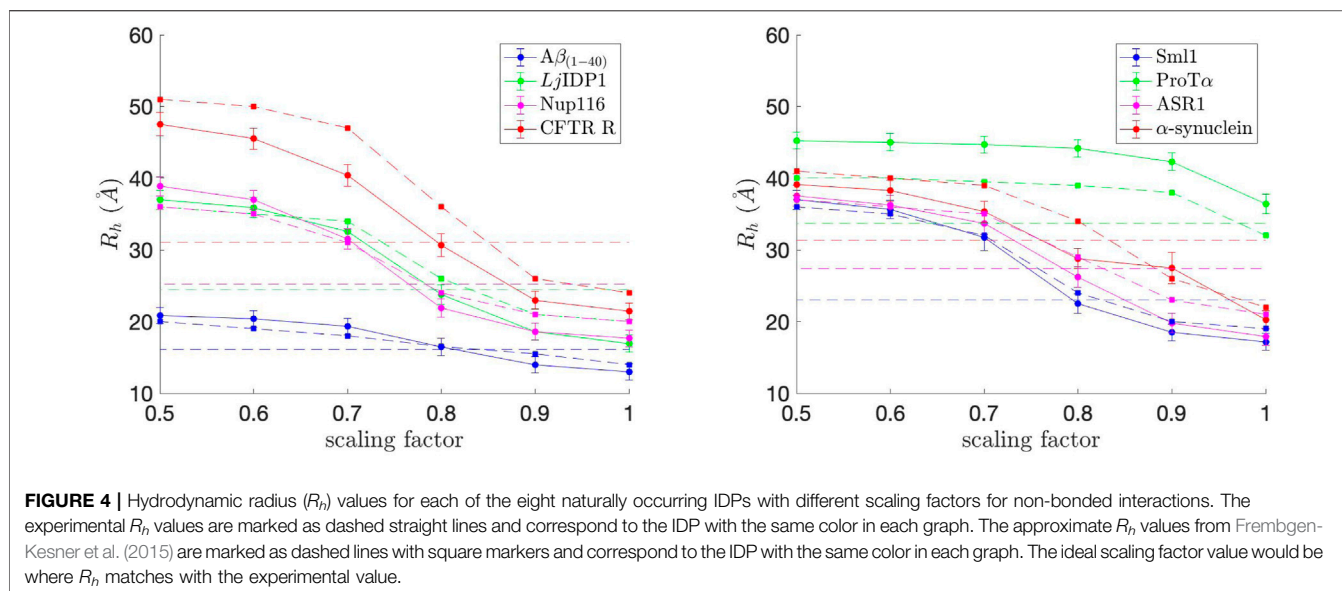


**FIGURE 4 |** Hydrodynamic radius ( $R_h$ ) values for each of the eight naturally occurring IDPs with different scaling factors for non-bonded interactions. The experimental  $R_h$  values are marked as dashed straight lines and correspond to the IDP with the same color in each graph. The approximate  $R_h$  values from Frembgen-Kesner et al. (2015) are marked as dashed lines with square markers and correspond to the IDP with the same color in each graph. The ideal scaling factor value would be where  $R_h$  matches with the experimental value.

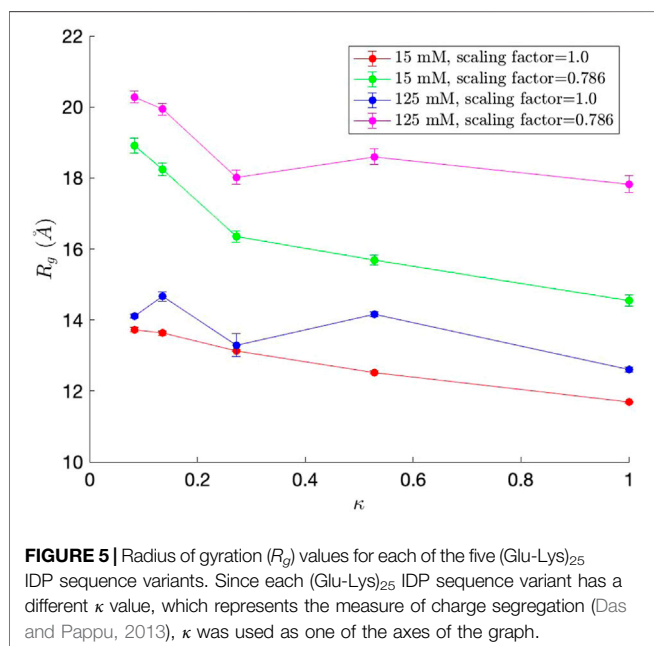


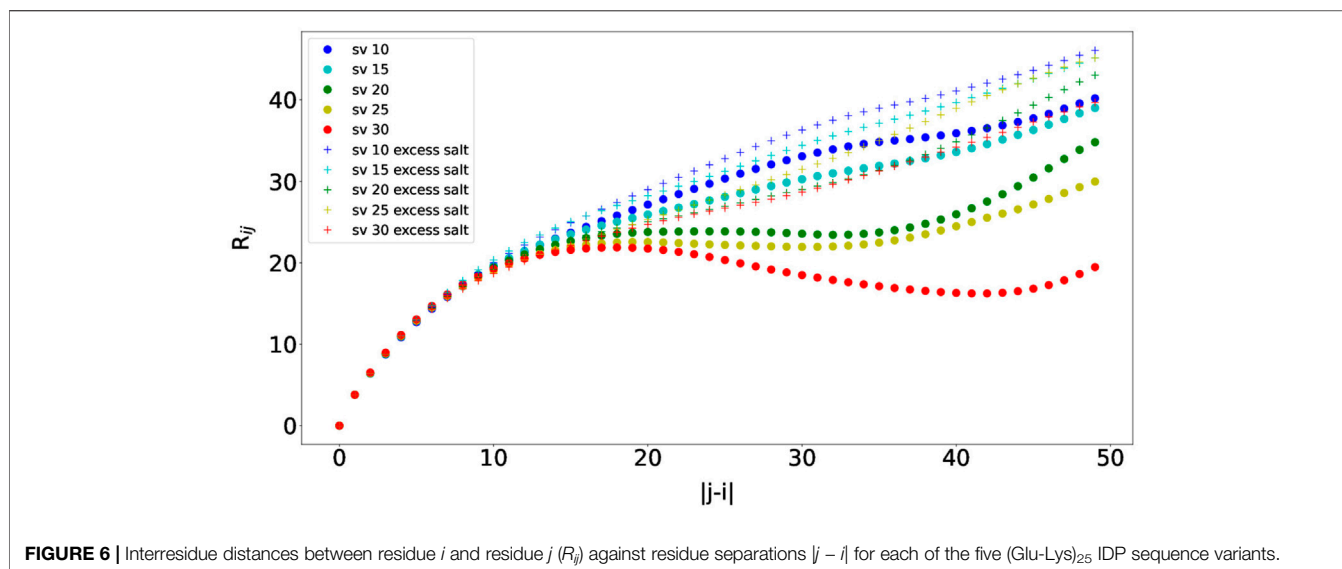
**FIGURE 5 |** Radius of gyration ( $R_g$ ) values for each of the five (Glu-Lys)<sub>25</sub> IDP sequence variants. Since each (Glu-Lys)<sub>25</sub> IDP sequence variant has a different  $\kappa$  value, which represents the measure of charge segregation (Das and Pappu, 2013),  $\kappa$  was used as one of the axes of the graph.

experimental values. We can consider ProT $\alpha$  to be an outlier among the eight naturally occurring IDPs since it substantially has more like-charged residues (i.e., positively charged residues aspartic acid (D) and glutamic acid (E)) as seen in **Figure 2** and as noted in Frembgen-Kesner et al. (2015). The averaged ideal scaling factor, after leaving ProT $\alpha$  out as an outlier, is 0.786, which is slightly different from the scaling factor in Frembgen-Kesner et al. (2015) (0.825). This scaling factor was used for subsequent COFFDROP BD simulations of the five (Glu-Lys)<sub>25</sub> IDP sequence variants. Finally, **Figure 4** shows that  $R_h$  generally increases with sequence length, except for ProT $\alpha$  that is shorter than ASR1, Nup116,  $\alpha$ -synuclein, and CFTR R.

### 3.2 Five (Glu-Lys)<sub>25</sub> IDP Sequence Variants

We then investigated five (Glu-Lys)<sub>25</sub> IDP sequence variants for rates of association, which were model IDP systems in Das and Pappu (2013), Sawle and Ghosh (2015), and McCarty et al. (2019). These block polymers of glutamate and lysine residues with different patterns serve as model IDPs since IDPs mostly consist of oppositely charged residues (i.e., they are polyampholytes) and do not have significant secondary structures.

We first measured the radius of gyration ( $R_g$ ), which serves as an indicator of protein structure compactness, i.e., the smaller the  $R_g$ , the tighter the packing of the protein is.  $R_g$  was calculated for each simulation snapshot (every 100,000 steps), and the final  $R_g$  value for each simulation was obtained by averaging the  $R_g$  values from the simulation. The average  $R_g$  values, along with standard error bars (95% confidence interval), from ten independent simulations, are plotted in **Figure 5**. As observed in Das and Pappu (2013),  $R_g$  generally decreases as  $\kappa$ , which represents the measure of charge segregation (Das and Pappu, 2013), increases. The  $R_g$  values are smaller than those from Das and Pappu (2013), all within the value for classical Flory random coils ( $\sim 18$  Å) and compact globules ( $\sim 11$  Å). The  $R_g$  values never reach near the value for self-avoiding random walks ( $\sim 28$  Å), which is expected for well-mixed sequence variants or those with low  $\kappa$  values. This is most likely attributed from using different force fields and potentially shows the limitation for the COFFDROP potential in modeling highly charged systems. However, when using the averaged ideal scaling factor for IDPs (0.786), the  $R_g$  values increase, show closer to expected  $R_g$  values, and its minimum  $R_g$  range match with that in Das and Pappu (2013). As  $\kappa \rightarrow 1$ , the  $R_g$  values get closer to the value for compact globules ( $\sim 11$  Å) (Dima and Thirumalai, 2004). Finally, the  $R_g$  values increase as the salt concentration increases due to long-range interactions getting weaker, which is consistent with the results from Das and Pappu (2013). Overall, we were able to observe correct trends for



$R_g$  for the five (Glu-Lys)<sub>25</sub> IDP sequence variants using the COFFDROP potential.

We then measured the interresidue distances between residue  $i$  and residue  $j$  ( $R_{ij}$ ) against residue separations  $|j - i|$ , which can characterize local concentrations of chain segments within the IDP (Das and Pappu, 2013). Specifically, the distance between residue  $i$ 's  $C_\alpha$  and residue  $j$ 's  $C_\alpha$  was measured. The scaling factor was set to the averaged ideal scaling factor of 0.786.  $R_{ij}$  was calculated for each simulation snapshot (every 100,000 steps), and the final  $R_{ij}$  value for each simulation was obtained by averaging the  $R_{ij}$  values from the simulation. The average  $R_{ij}$  values from ten independent simulations are plotted in **Figure 6**. The  $R_{ij}$  values follow similar trends as observed in Das and Pappu (2013), and the concave upward parts show indications of long-range interactions between oppositely charged blocks. As observed for the  $R_g$  values, the  $R_{ij}$  values were also smaller than those from Das and Pappu (2013), which could be attributed from using different force fields. Finally, the  $R_{ij}$

values also increase as the salt concentration increases due to long-range interactions getting weaker, which is consistent with the results from Das and Pappu (2013). The effects of the salt concentration are the smallest for sv10, which has the most well-mixed sequence in comparison with the rest and can counterbalance electrostatic repulsions and attractions (Das and Pappu, 2013). Overall, we were also able to observe correct trends with  $R_{ij}$  for the five (Glu-Lys)<sub>25</sub> IDP sequence variants using the COFFDROP potential.

Finally, we measured a property related to molecular association, namely the entanglement indices, or the average  $C_\alpha$  distances to the other chain, between the five (Glu-Lys)<sub>25</sub> IDP sequence variants. Since all possible pair combinations were tested, 15 simulations were run for each salt concentration (15 and 125 mM, respectively). The scaling factor was set to the averaged ideal scaling factor of 0.786. The pairwise simulations start with two IDP sequence variants oriented crosswise and translated 15 Å apart. All five IDP sequence variants have their

**TABLE 2** | Summary of entanglement index values of all possible pair combinations between the five (Glu-Lys)<sub>25</sub> IDP sequence variants.

IDP #1	IDP #2	Entanglement index (Å) at 15 mM	Entanglement index (Å) at 125 mM
sv10	sv10	26.72 ± 0.98	26.38 ± 0.58
sv10	sv15	25.93 ± 0.63	27.12 ± 0.39
sv10	sv20	26.54 ± 0.98	26.70 ± 0.49
sv10	sv25	26.72 ± 0.71	26.92 ± 0.50
sv10	sv30	25.43 ± 1.61	26.70 ± 1.21
sv15	sv15	26.72 ± 0.53	27.68 ± 0.44
sv15	sv20	25.72 ± 0.69	27.29 ± 0.18
sv15	sv25	26.58 ± 0.75	26.87 ± 1.10
sv15	sv30	26.17 ± 0.28	27.98 ± 0.81
sv20	sv20	25.48 ± 0.31	25.78 ± 0.56
sv20	sv25	26.89 ± 0.83	25.85 ± 0.57
sv20	sv30	26.07 ± 0.31	26.38 ± 0.70
sv25	sv25	27.00 ± 0.25	27.44 ± 0.58
sv25	sv30	25.07 ± 3.05	27.15 ± 0.40
sv30	sv30	24.17 ± 2.38	26.59 ± 0.81

middle  $C_{\alpha}$  centered at (0.0, 0.0, 0.0). The middle  $C_{\alpha}$ 's of the two IDP sequence variants in the pairwise simulation were restrained to be less than 20 Å apart. The entanglement indices were measured using the `entanglement_index`, which is a new implementation in BrownDye 2.0. The entanglement index was calculated for each simulation snapshot (every 100,000 steps), and the final entanglement index for each simulation was obtained by averaging the entanglement indices from the simulation. The average entanglement indices, along with standard error bars (95% confidence interval), from ten independent simulations are listed in **Table 2**. The entanglement indices were similar across all possible IDP sequence variant pairs, indicating that there is no direct relation between entanglement indices and charge segregation  $\kappa$ . This may be from all sequence variants having relatively similar  $R_g$  values or degrees of compactness, however, which could be from using the COFFDROP potential. All entanglement indices, with the exception for two pairs, increased, however, at excess salt concentration. This is consistent with long-range interactions getting weaker at increasing salt concentration, and published work demonstrating that long-range interactions accelerate protein-protein encounter for IDPs (Chu et al., 2012; Ganguly et al., 2013; Pang and Zhou, 2016; Tsai et al., 2016; Chu et al., 2017; Yang et al., 2019).

## 4 DISCUSSION AND CONCLUSION

We have presented our new COFFDROP force field implementation on BrownDye 2.0 that enabled us to study IDPs computationally. BD simulations are ideal to study large-scale motions with longer time scales and diffusion-limited molecular associations, including the aggregation of IDPs. We have presented results that show that our COFFDROP implementation is reliable to study naturally occurring IDPs. We have also studied model (Glu-Lys)<sub>25</sub> IDPs using our COFFDROP implementation and found that there is no relation between entanglement indices and how well the charges are mixed and segregated within the IDPs. However, this may be from the limitation of the COFFDROP potential in studying highly charged systems, which was also noted in Frembgen-Kesner et al. (2015). The COFFDROP potential was derived from MD simulations of all possible amino acid pairs (Andrews and Elcock, 2014; Frembgen-Kesner et al., 2015), but the simulations did not include salt so the COFFDROP potential may be limiting in modeling systems with strong charge-charge interactions.

For future work, we plan to implement a program to measure the rates of association with an appropriate reaction criterion as done in Ganguly et al. (2013), Liu et al. (2019). Then we plan to measure the rates of association of a highly positive IDP binding

to a highly negative IDP (i.e., oppositely charged IDPs), an interaction that may be abundant in eukaryotes for regulation (e.g., cellular localization) (Borgia et al., 2018). We also plan to look at the rates of association between IDPs and folded proteins with secondary structures (Ruff et al., 2019). However, since COFFDROP is meant to model IDPs or systems without significant secondary or tertiary structures, the secondary structural elements would need to have constraints to have them fixed throughout the simulation, and the folded protein would be treated as a rigid body. The IDP would still be modeled as a flexible chain, and the scaling factor of 0.786 would be used for the simulation.

## DATA AVAILABILITY STATEMENT

The original contributions presented in the study are included in the article/**Supplementary Material**, further inquiries can be directed to the corresponding author.

## AUTHOR CONTRIBUTIONS

S-HA: Conceptualization, investigation, methodology, data curation, validation, writing- original draft preparation. GH: Investigation, methodology, data curation, validation, writing-reviewing and editing. JM: Conceptualization, methodology, writing- reviewing and editing, supervision, funding acquisition.

## FUNDING

S-HA and GH acknowledge support from NIH GM31749 and University of California, San Diego.

## ACKNOWLEDGMENTS

All simulations were done using the Triton Shared Computing Cluster (TSCC) at the San Diego Supercomputing Center (SDSC). The authors thank Adrian Elcock for giving helpful suggestions.

## SUPPLEMENTARY MATERIAL

The Supplementary Material for this article can be found online at: <https://www.frontiersin.org/articles/10.3389/fmolb.2022.898838/full#supplementary-material>

## REFERENCES

Alberts, B., Johnson, A., Lewis, J., Raff, M., Roberts, K., and Walter, P. (2002). *Molecular Biology of the Cell*. Fourth Edition. New York: Garland Science.

Alderson, T. R., Pritišanac, I., Moses, A. M., and Forman-Kay, J. D. (2022). Systematic Identification of Conditionally Folded Intrinsically Disordered Regions by AlphaFold2. *bioRxiv*. doi:10.1101/2022.02.18.481080

Andrews, C. T., and Elcock, A. H. (2014). Coffdrop: a Coarse-Grained Nonbonded Force Field for Proteins Derived from All-Atom Explicit-Solvent Molecular



- Dynamics Simulations of Amino Acids. *J. Chem. Theory Comput.* 10, 5178–5194. doi:10.1021/ct5006328
- Baker, J. M. R. (2009). *Structural Characterization and Interactions of the CFTR Regulatory Region*. Toronto, Canada: University of Toronto.
- Borgia, A., Borgia, M. B., Bugge, K., Kissling, V. M., Heidarsson, P. O., Fernandes, C. B., et al. (2018). Extreme Disorder in an Ultrahigh-Affinity Protein Complex. *Nature* 555, 61–66. doi:10.1038/nature25762
- Chu, W.-T., Clarke, J., Shammas, S. L., and Wang, J. (2017). Role of Non-native Electrostatic Interactions in the Coupled Folding and Binding of Puma with Mcl-1. *PLoS Comput. Biol.* 13, e1005468. doi:10.1371/journal.pcbi.1005468
- Chu, X., Wang, Y., Gan, L., Bai, Y., Han, W., Wang, E., et al. (2012). Importance of Electrostatic Interactions in the Association of Intrinsically Disordered Histone Chaperone Chz1 and Histone H2A.Z-H2b. *PLoS Comput. Biol.* 8, e1002608. doi:10.1371/journal.pcbi.1002608
- Danielsson, J., Jarvet, J., Damberg, P., and Gräslund, A. (2002). Translational Diffusion Measured by PFG-NMR on Full Length and Fragments of the Alzheimer A $\beta$ (1-40) Peptide. Determination of Hydrodynamic Radii of Random Coil Peptides of Varying Length. *Magn. Reson. Chem.* 40, S89–S97. doi:10.1002/mrc.1132
- Danielsson, J., Liljedahl, L., Bárányi-Wallje, E., Sönderby, P., Kristensen, L. H., Martínez-Yamout, M. A., et al. (2008). The Intrinsically Disordered Rnr Inhibitor Sml1 Is a Dynamic Dimer. *Biochemistry* 47, 13428–13437. doi:10.1021/bi801040b
- Das, R. K., and Pappu, R. V. (2013). Conformations of Intrinsically Disordered Proteins Are Influenced by Linear Sequence Distributions of Oppositely Charged Residues. *Proc. Natl. Acad. Sci. U.S.A.* 110, 13392–13397. doi:10.1073/pnas.1304749110
- Dima, R. I., and Thirumalai, D. (2004). Asymmetry in the Shapes of Folded and Denatured States of Proteins. *J. Phys. Chem. B* 108, 6564–6570. doi:10.1021/jp037128y
- Dolinsky, T. J., Czodrowski, P., Li, H., Nielsen, J. E., Jensen, J. H., Klebe, G., et al. (2007). Pdb2pqr: Expanding and Upgrading Automated Preparation of Biomolecular Structures for Molecular Simulations. *Nucleic Acids Res.* 35, W522–W525. doi:10.1093/nar/gkm276
- Dolinsky, T. J., Nielsen, J. E., McCammon, J. A., and Baker, N. A. (2004). PDB2PQR: an Automated Pipeline for the Setup of Poisson-Boltzmann Electrostatics Calculations. *Nucleic Acids Res.* 32, W665–W667. doi:10.1093/nar/gkh381
- Elcock, A. H. (2004). “Molecular Simulations of Diffusion and Association in Multimacromolecular Systems,” in *Numerical Computer Methods, Part D. Vol. 383 of Methods in Enzymology* (Cambridge, MA, USA: Academic Press), 166–198. doi:10.1016/s0076-6879(04)83008-8
- Elcock, A. H. (2013). Molecule-centered Method for Accelerating the Calculation of Hydrodynamic Interactions in Brownian Dynamics Simulations Containing Many Flexible Biomolecules. *J. Chem. Theory Comput.* 9, 3224–3239. doi:10.1021/ct400240w
- Frembgen-Kesner, T., Andrews, C. T., Li, S., Ngo, N. A., Shubert, S. A., Jain, A., et al. (2015). Parametrization of Backbone Flexibility in a Coarse-Grained Force Field for Proteins (Coffdrop) Derived from All-Atom Explicit-Solvent Molecular Dynamics Simulations of All Possible Two-Residue Peptides. *J. Chem. Theory Comput.* 11, 2341–2354. doi:10.1021/acs.jctc.5b00038
- Ganguly, D., Zhang, W., and Chen, J. (2013). Electrostatically Accelerated Encounter and Folding for Facile Recognition of Intrinsically Disordered Proteins. *PLoS Comput. Biol.* 9, e1003363. doi:10.1371/journal.pcbi.1003363
- Goldgur, Y., Rom, S., Ghirlando, R., Shkolnik, D., Shadrin, N., Konrad, Z., et al. (2007). Desiccation and Zinc Binding Induce Transition of Tomato Abscisic Acid Stress Ripening 1, a Water Stress- and Salt Stress-Regulated Plant-specific Protein, from Unfolded to Folded State. *Plant Physiol.* 143, 617–628. doi:10.1104/pp.106.092965
- Grant, B. J., M. Gheorghe, D., Zheng, W., Alonso, M., Huber, G., Dlugosz, M., et al. (2011). Electrostatically Biased Binding of Kinesin to Microtubules. *PLoS Biol.* 9, e1001207. doi:10.1371/journal.pbio.1001207
- Haaning, S., Radutoiu, S., Hoffmann, S. V., Dittmer, J., Giehm, L., Otzen, D. E., et al. (2008). An Unusual Intrinsically Disordered Protein from the Model Legume lotus Japonicus Stabilizes Proteins *In Vitro*. *J. Biol. Chem.* 283, 31142–31152. doi:10.1074/jbc.m805024200
- Holehouse, A. S., Ahad, J., Das, R. K., and Pappu, R. V. (2015). Cider: Classification of Intrinsically Disordered Ensemble Regions. *Biophysical J.* 108, 228a. doi:10.1016/j.bpj.2014.11.1260
- Huang, Y.-m. M., Huber, G. A., Wang, N., Miteer, S. D., and McCammon, J. A. (2018). Brownian Dynamic Study of an Enzyme Metabolon in the Tca Cycle: Substrate Kinetics and Channeling. *PROTEIN Sci.* 27, 463–471. doi:10.1002/pro.3338
- Huber, G. A., and McCammon, J. A. (2010). Browndye: a Software Package for Brownian Dynamics. *Comput. Phys. Commun.* 181, 1896–1905. doi:10.1016/j.cpc.2010.07.022
- Huber, G. A., and McCammon, J. A. (2019). Brownian Dynamics Simulations of Biological Molecules. *Trends Chem.* 1, 727–738. doi:10.1016/j.trechm.2019.07.008
- Iqbalsyah, T. M., and Doig, A. J. (2005). Anticooperativity in a Glu–Lys–Glu Salt Bridge Triplet in an Isolated  $\alpha$ -Helical Peptide. *Biochemistry* 44, 10449–10456. doi:10.1021/bi0508690
- Jumper, J., Evans, R., Pritzel, A., Green, T., Figurnov, M., Ronneberger, O., et al. (2021). Highly Accurate Protein Structure Prediction with AlphaFold. *Nature* 596, 583–589. doi:10.1038/s41586-021-03819-2
- Jurrus, E., Engel, D., Star, K., Monson, K., Brandi, J., Felberg, L. E., et al. (2018). Improvements to the Apbs Biomolecular Solvation Software Suite. *Protein Sci.* 27, 112–128. doi:10.1002/pro.3280
- Kirkwood, J. G. (1996). The General Theory of Irreversible Processes in Solutions of Macromolecules. *J. Polym. Sci. B Polym. Phys.* 34, 597–610. doi:10.1002/polb.1996.897
- Krishnan, V. V., Lau, E. Y., Yamada, J., Denning, D. P., Patel, S. S., Colvin, M. E., et al. (2008). Intramolecular Cohesion of Coils Mediated by Phenylalanine-Glycine Motifs in the Natively Unfolded Domain of a Nucleoporin. *PLoS Comput. Biol.* 4, e1000145. doi:10.1371/journal.pcbi.1000145
- Kyte, J., and Doolittle, R. F. (1982). A Simple Method for Displaying the Hydrophobic Character of a Protein. *J. Mol. Biol.* 157, 105–132. doi:10.1016/0022-2836(82)90515-0
- Li, P., Johnston, H., and Krasny, R. (2009). A Cartesian Treecode for Screened Coulomb Interactions. *J. Comput. Phys.* 228, 3858–3868. doi:10.1016/j.jcp.2009.02.022
- Liu, X., Chen, J., and Chen, J. (2019). Residual Structure Accelerates Binding of Intrinsically Disordered Actr by Promoting Efficient Folding upon Encounter. *J. Mol. Biol.* 431, 422–432. doi:10.1016/j.jmb.2018.12.001
- Marqusee, S., and Baldwin, R. L. (1987). Helix Stabilization by Glu-Lys+ Salt Bridges in Short Peptides of De Novo Design. *Proc. Natl. Acad. Sci. U.S.A.* 84, 8898–8902. doi:10.1073/pnas.84.24.8898
- Martinez, M., Bruce, N. J., Romanowska, J., Kokh, D. B., Ozybayraci, M., Yu, X., et al. (2015). Sda 7: A Modular and Parallel Implementation of the Simulation of Diffusional Association Software. *J. Comput. Chem.* 36, 1631–1645. doi:10.1002/jcc.23971
- McCarty, J., Delaney, K. T., Danielsen, S. P. O., Fredrickson, G. H., and Shea, J.-E. (2019). Complete Phase Diagram for Liquid-Liquid Phase Separation of Intrinsically Disordered Proteins. *J. Phys. Chem. Lett.* 10, 1644–1652. doi:10.1021/acs.jpclett.9b00099
- Meuzelaar, H., Vreede, J., and Woutersen, S. (2016). Influence of Glu/Arg, Asp/Arg, and Glu/Lys Salt Bridges on  $\alpha$ -Helical Stability and Folding Kinetics. *Biophysical J.* 110, 2328–2341. doi:10.1016/j.bpj.2016.04.015
- Northrup, S. H., Thomasson, K. A., Miller, C. M., Barker, P. D., Eltis, L. D., Guillet, J. G., et al. (1993). Effects of Charged Amino Acid Mutations on the Bimolecular Kinetics of Reduction of Yeast Iso-1-Ferricytochrome C by Bovine Ferrocyclochrome B5. *Biochemistry* 32, 6613–6623. doi:10.1021/bi00077a014
- Nygaard, M., Kragelund, B. B., Papaleo, E., and Lindorff-Larsen, K. (2017). An Efficient Method for Estimating the Hydrodynamic Radius of Disordered Protein Conformations. *Biophysical J.* 113, 550–557. doi:10.1016/j.bpj.2017.06.042
- Olsson, M. H. M., Sondergaard, C. R., Rostkowski, M., and Jensen, J. H. (2011). PROPKA3: Consistent Treatment of Internal and Surface Residues in Empirical pKa Predictions. *J. Chem. Theory Comput.* 7, 525–537. doi:10.1021/ct100578z
- Ortega, A., Amorós, D., and García de la Torre, J. (2011). Prediction of Hydrodynamic and Other Solution Properties of Rigid Proteins from

- Atomic- and Residue-Level Models. *Biophysical J.* 101, 892–898. doi:10.1016/j.bpj.2011.06.046
- Pang, X., and Zhou, H.-X. (2016). Mechanism and Rate Constants of the Cdc42 Gtpase Binding with Intrinsically Disordered Effectors. *Proteins* 84, 674–685. doi:10.1002/prot.25018
- Pollard, T., and Earnshaw, W. (2007). *Cell Biology*. New York: W.B. Saunders.
- Roberts, C. C., and Chang, C.-e. A. (2016). Analysis of Ligand-Receptor Association and Intermediate Transfer Rates in Multienzyme Nanostructures with All-Atom Brownian Dynamics Simulations. *J. Phys. Chem. B* 120, 8518–8531. doi:10.1021/acs.jpcc.6b02236
- Ruff, K. M., Pappu, R. V., and Holehouse, A. S. (2019). Conformational Preferences and Phase Behavior of Intrinsically Disordered Low Complexity Sequences: Insights from Multiscale Simulations. *Curr. Opin. Struct. Biol.* 56, 1–10. doi:10.1016/j.sbi.2018.10.003
- Ryckaert, J.-P., Ciccotti, G., and Berendsen, H. J. C. (1977). Numerical Integration of the Cartesian Equations of Motion of a System with Constraints: Molecular Dynamics of N-Alkanes. *J. Comput. Phys.* 23, 327–341. doi:10.1016/0021-9991(77)90098-5
- Sawle, L., and Ghosh, K. (2015). A Theoretical Method to Compute Sequence Dependent Configurational Properties in Charged Polymers and Proteins. *J. Chem. Phys.* 143, 085101. doi:10.1063/1.4929391
- Søndergaard, C. R., Olsson, M. H., Rostkowski, M., and Jensen, J. H. (2011). Improved Treatment of Ligands and Coupling Effects in Empirical Calculation and Rationalization of pKa Values. *J. Chem. Theory Comput.* 7, 2284–2295. doi:10.1021/ct200133y
- Tsai, M.-Y., Zheng, W., Balamurugan, D., Schafer, N. P., Kim, B. L., Cheung, M. S., et al. (2016). Electrostatics, Structure Prediction, and the Energy Landscapes for Protein Folding and Binding. *Protein Sci.* 25, 255–269. doi:10.1002/pro.2751
- Unni, S., Huang, Y., Hanson, R. M., Tobias, M., Krishnan, S., Li, W. W., et al. (2011). Web Servers and Services for Electrostatics Calculations with Apbs and Pdb2pqr. *J. Comput. Chem.* 32, 1488–1491. doi:10.1002/jcc.21720
- Uversky, V. N., Lee, H.-J., Li, J., Fink, A. L., and Lee, S.-J. (2001). Stabilization of Partially Folded Conformation during  $\alpha$ -Synuclein Oligomerization in Both Purified and Cytosolic Preparations. *J. Biol. Chem.* 276, 43495–43498. doi:10.1074/jbc.c100551200
- Uversky, V. N. (2002). Natively Unfolded Proteins: a Point where Biology Waits for Physics. *Protein Sci.* 11, 739–756. doi:10.1110/ps.4210102
- Wolny, M., Batchelor, M., Bartlett, G. J., Baker, E. G., Kurzawa, M., Knight, P. J., et al. (2017). Characterization of Long and Stable De Novo Single Alpha-Helix Domains Provides Novel Insight into Their Stability. *Sci. Rep.* 7, 44341–44414. doi:10.1038/srep44341
- Yang, J., Gao, M., Xiong, J., Su, Z., and Huang, Y. (2019). Features of Molecular Recognition of Intrinsically Disordered Proteins via Coupled Folding and Binding. *Protein Sci.* 28, 1952–1965. doi:10.1002/pro.3718
- Yi, S., Boys, B. L., Brickenden, A., Konermann, L., and Choy, W.-Y. (2007). Effects of Zinc Binding on the Structure and Dynamics of the Intrinsically Disordered Protein Prothymosin  $\alpha$ : Evidence for Metalation as an Entropic Switch. *Biochemistry* 46, 13120–13130. doi:10.1021/bi7014822
- Zuk, P. J., Wajnryb, E., Mizerski, K. A., and Szymczak, P. (2014). Rotne-prager-yamakawa Approximation for Different-Sized Particles in Application to Macromolecular Bead Models. *J. Fluid Mech.* 741, 668. doi:10.1017/jfm.2013.668

**Conflict of Interest:** The authors declare that the research was conducted in the absence of any commercial or financial relationships that could be construed as a potential conflict of interest.

**Publisher's Note:** All claims expressed in this article are solely those of the authors and do not necessarily represent those of their affiliated organizations, or those of the publisher, the editors and the reviewers. Any product that may be evaluated in this article, or claim that may be made by its manufacturer, is not guaranteed or endorsed by the publisher.

Copyright © 2022 Ahn, Huber and McCammon. This is an open-access article distributed under the terms of the Creative Commons Attribution License (CC BY). The use, distribution or reproduction in other forums is permitted, provided the original author(s) and the copyright owner(s) are credited and that the original publication in this journal is cited, in accordance with accepted academic practice. No use, distribution or reproduction is permitted which does not comply with these terms.